Journal of Sound and Vibration (2002) **253**(2), 471–483
doi:10.1006/jsvi.2001.4063, available online at http://www.idealibrary.com on IDEAL®

NON-LINEAR AEROELASTIC ANALYSIS USING THE POINT TRANSFORMATION METHOD, PART 2: HYSTERESIS MODEL

L. LIU† AND Y. S. WONG

Department of Mathematical Sciences, University of Alberta, Edmonton, Alta., Canada T6G 2G1.
E-mail: lliu@math.ualberta.ca

AND

B. H. K. LEE
Institute for Aerospace Research, National Research Council, Ottawa, Ont., Canada K1A 0R6

(*Received* 6 *March* 2001, *and in final form* 20 *September* 2001)

This paper investigates the dynamic response of a two-dimensional aeroelastic system with structural non-linearity represented by hysteresis. The formulations of the point transformation method developed in Part 1 of this study for the aeroelastic system with a freeplay model is extended for a hysteresis model. These formulations can be applied not only to predict the amplitude and frequency of limit cycle oscillations, but also to detect complex aeroelastic responses such as periodic motion with harmonics, period doubling, chaotic motion and the coexistence of stable limit cycles. It is shown that the point transformation technique is the most suitable to analyze the aeroelastic response of systems containing piecewise continuous restoring forces.

1. INTRODUCTION

Non-linear aeroelasticity involves non-linear aerodynamics and non-linear structures. There are three types of non-linearities in concentrated non-linear structures, namely cubic, freeplay and hysteresis stiffnesses. The describing function [1], harmonic balance method [2], the center manifold and the principle of normal form [3] have been successfully used to analyze aeroelastic systems with cubic stiffnesses. The describing function method [4] and the rational polynomial approximation for the freeplay model [5] were applied to analyze the aeroelastic system with a freeplay model. This paper extends the point transformation technique developed in Part 1 of this study for freeplay models to investigate the dynamic response of the aeroelastic system with a hysteresis model.

Compared to the study of cubic and freeplay non-linearities, much less literature has been found on the study of hysteresis non-linearity. The first attempt to study such effects in aeroelasticity was carried out by Woolston *et al.* [6], who numerically determined the flutter boundaries for a two-dimensional airfoil placed in an incompressible flow. Some examples were re-examined by Shen and Hsu [7] and Shen [1] using the describing function method. This method was also used by Breitbach [8] to analyze aircraft structures with hysteresis. A numerical simulation using the fourth order Runge–Kutta time-integration scheme was carried out in a recent study by Chan [9]. Only a hysteresis

†Present address: Institute for Aerospace Research, Uplands, U-66, National Research Council, Ottawa, ON, Canada K1A 0R6. E-mail: liping.liu@nrc.ca.

0022-460X/02/$35.00

non-linearity in the pitch degree of freedom (d.o.f.) was considered, and 19 cases were carefully studied for various system parameters and hysteresis constants. The flutter boundary diagram obtained by Chan [9] is similar to that in Woolston *et al.* [6], but the numerical simulations give more details on the boundary curves and the existence of isolated pockets of limit cycle oscillations (LCOs) inside the main flutter boundary. The flutter boundary shows that the oscillations become divergent for velocity ratios larger than 1. In the main LCO region, the motion seems to be a simple sinusoid with a fundamental harmonic. This shows that the assumption of a dominant frequency in the harmonic balance or describing function technique is reasonable for motions in this LCO region. However, inside one of the LCO pockets, the presence of higher harmonics is clearly noticeable, which suggests the possible failure of Shen's [1] harmonic balance analysis for these motions.

Since the hysteresis non-linearity can be represented by a superposition of two freeplays, the location of switching points and the initial conditions are as important as they are in the freeplay model. As a piecewise linear system, a hysteresis model can also be analyzed by the point transformation method. Unlike a freeplay model with only three linear subsystems, a hysteresis model consists of six linear subsystems governing six regions in its state space. However, because of the special charcteristics of a symmetric hysteresis model, at most four switching points are actually needed to locate for one loop of the motion. Two formulations of the point transformation method are now developed for this hysteresis model by extending Part 1 of this study [10] for a freeplay model. Applications of these formulations to several examples are carried out to study the non-linear behavior of the model, whose results confirm most of Chan's [9] numerical solutions. Furthermore, the point transformation technique not only detects the existence of the period-one, period-two, and period-four LCOs with harmonics components, but it is also capable of predicting the amplitudes and frequencies of these motions. This point transformation method with attractive features such as taking into account the initial conditions and locating the switching points exactly is the most suitable analytical method for investigating the aeroelastic response of systems containing piecewise linear restoring forces.

Similar to the numerical scheme for a freeplay model, the time-integration scheme for the hysteresis model cannot be proved to be stable since some of the eigenvalues corresponding to the linear subsystems may have positive real parts. Furthermore, the scheme cannot precisely locate the switching points where the change in linear regions occurs. However, for the cases reported in this paper, the numerical solutions obtained by using the Runge–Kutta method are accurate since the chosen time steps are sufficiently small. Thus, in the result and discussion section, the numerical results are used to cross check the predictions obtained by the point transformation method.

In Part 1 of this study, the original two-dimensional airfoil motion without any external forces has been rewritten into a system of the first order ordinary differential equations

$$
\begin{aligned}
x_1' &= x_2,\\
x_2' &= a_{21}x_1 + a_{22}x_2 + a_{23}x_3 + a_{24}x_4 + a_{25}x_5 + a_{26}x_6 + a_{27}x_7\\
&\quad + a_{28}x_8 + j\left(d_0\left(\frac{\bar{\omega}}{U^*}\right)^2 G(x_3) - c_0\left(\frac{1}{U^*}\right)^2 M(x_1)\right),\\
x_3' &= x_4,\\
x_4' &= a_{41}x_1 + a_{42}x_2 + a_{43}x_3 + a_{44}x_4 + a_{45}x_5 + a_{46}x_6 + a_{47}x_7\\
&\quad + a_{48}x_8 + j\left(c_1\left(\frac{1}{U^*}\right)^2 M(x_1) - d_1\left(\frac{\bar{\omega}}{U^*}\right)^2 G(x_3)\right),\\
x_5' &= x_1 - \varepsilon_1 x_5, \qquad x_6' = x_1 - \varepsilon_2 x_6, \qquad x_7' = x_3 - \varepsilon_1 x_7, \qquad x_8' = x_3 - \varepsilon_2 x_8
\end{aligned}
\tag{1}
$$

with all the notations given in Part 1 of this study [10] and the appendices therein. The structural non-linearities are represented by the non-linear functions $G(x_3)$ and $M(x_1)$.

For a hysteresis stiffness, $M(x_1)$ is given by

$$M(x_1) = \begin{cases} x_1 - \alpha_f + M_0, & x_1 < \alpha_f \uparrow, \\ x_1 + \alpha_f - M_0, & x_1 > -\alpha_f \downarrow, \\ M_0, & \alpha_f \leqslant x_1 \leqslant \alpha_f + \delta \uparrow, \\ -M_0, & -\alpha_f - \delta \leqslant x_1 \leqslant -\alpha_f \downarrow, \\ x_1 - \alpha_f - \delta + M_0, & x_1 > \alpha_f + \delta \uparrow, \\ x_1 + \alpha_f + \delta - M_0, & x_1 < -\alpha_f - \delta \downarrow, \end{cases} \tag{2}$$

where $\uparrow$ and $\downarrow$ represent the motion in the increasing and decreasing x_1 direction respectively. M_0, α_f and δ are constants. Here, we give the expressions for $M(x_1)$ in the pitch d.o.f.; similar expressions for $G(x_3)$ in the plunge motion can be written by replacing x_1 with x_3.

2. THE POINT TRANSFORMATION METHOD

A hysteresis model is a piecewise linear system whose state space consists of several linear regions, each of which is governed by a linear subsystem. The point transformation method, which is suitable for all piecewise linear systems, can be applied to this model. In this section, a general implementation of the point transformation technique is described first for the hysteresis model. Then, based on the general ideas, two formulations, similar to Part 1 of this study, are developed for the model. The applications of these formulations to several test examples are given in the next section.

Consider a hysteresis model given by equation (2). As x_1 increases, the system follows the upper branch of the hysteresis:

$$M(x_1) = \begin{cases} x_1 - \alpha_f + M_0, & x_1 < \alpha_f, \\ M_0, & \alpha_f \leqslant x_1 \leqslant \alpha_f + \delta, \\ x_1 - \alpha_f - \delta + M_0, & x_1 > \alpha_f + \delta. \end{cases}$$

On the other hand, as x_1 decreases, the system follows the lower branch of the hysteresis:

$$M(x_1) = \begin{cases} x_1 + \alpha_f + \delta - M_0, & x_1 < -\alpha_f - \delta, \\ -M_0, & -\alpha_f - \delta \leqslant x_1 \leqslant -\alpha_f, \\ x_1 + \alpha_f - M_0, & x_1 > -\alpha_f. \end{cases}$$

Thus, a hysteresis can be treated as two bilinear systems following specified directions. Without loss of generality, let $2\alpha_f + \delta = 2M_0$; we then have $x_1 - \alpha_f + M_0 = x_1 + \alpha_f + \delta - M_0$ and $x_1 - \alpha_f - \delta + M_0 = x_1 + \alpha_f - M_0$ and the sketch of the hysteresis stiffness is as shown in Figure 1. For this hysteresis model, as x_1 increases, the state space consists of three linear regions IR_i ($i = 1, 2, 3$), each of which corresponds to a linear subsystem,

$$\begin{aligned} IR_1 &= \{X \in R^8 | x_1 < \alpha_f\}: \quad X' = AX + F_1, \\ IR_2 &= \{X \in R^8 | \alpha_f \leqslant x_1 \leqslant \alpha_f + \delta\}: \quad X' = CX + F_4, \\ IR_3 &= \{X \in R^8 | x_1 > \alpha_f + \delta\}: \quad X' = AX - F_1. \end{aligned}$$

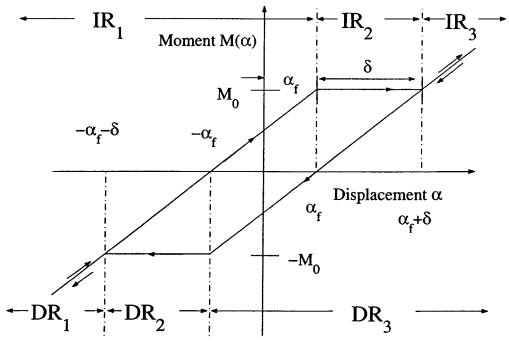

Figure 1. General sketch of a hysteresis stiffness.

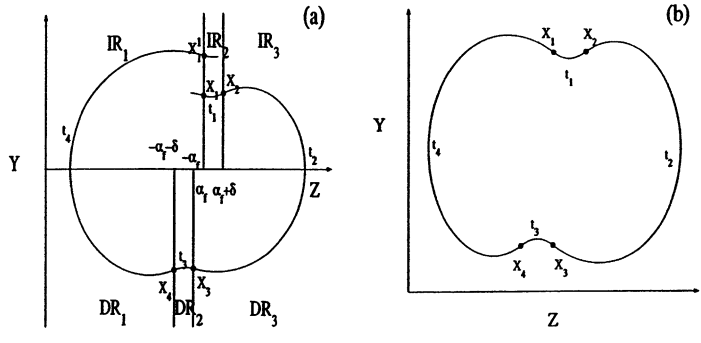

Figure 2. General trajectory (a) and a period-one LCO (b) of the aeroelastic system (1) with hysteresis structure; ●, switching points.

Similarly, as x_1 decreases, the three linear regions $DR_i (i = 1, 2, 3)$ of the state space are given by

$$DR_1 = \{X \in R^8 | x_1 < -\alpha_f - \delta\}: \quad X' = AX + F_1,$$
$$DR_2 = \{X \in R^8 | -\alpha_f - \delta \leqslant x_1 \leqslant -\alpha_f\}: \quad X' = CX - F_4,$$
$$DR_3 = \{X \in R^8 | x_1 > -\alpha_f\}: \quad X' = AX - F_1.$$

Here A and C are 8×8 constant matrices, and F_1 and F_4 are 8×1 constant vectors. The elements of A, C and F_i, $i = 1, 4$ are determined from the system parameters of the coupled aeroelastic equations, and they are given by

$$A = \begin{pmatrix} A_1 & A_2 \\ A_3 & A_4 \end{pmatrix}, \qquad C = \begin{pmatrix} C_1 & A_2 \\ A_3 & A_4 \end{pmatrix}$$

and $F_1 = (M_0 - \alpha_f)F$, $F_4 = M_0 F$, where the elements of the 4×4 block matrices for A_1, A_2, A_3, A_4 and the 8×1 vector F are defined in reference [11], and C_1 is given in Appendix A.

Let the Z–Y plane represent the eight-dimensional state space with $Z = \{x_1\}$ and $Y = \{x_2, x_3, x_4, x_5, x_6, x_7, x_8\}$. Then the Z–Y plane is divided by the subspaces $Z = -\alpha_f$, $Z = -\alpha_f - \delta$, $Z = \alpha_f$ and $Z = \alpha_f + \delta$ into six regions IR_1, IR_2, IR_3, DR_1, DR_2, and DR_3 as shown in Figure 2(a). From the general idea of the point transformation method, similar to the discussion for a freeplay model [10], six switching points are needed to be located for each loop of the motion. However, from the following discussion, only four of them are

important. Along with the upper branch of a hysteresis as shown in Figure 1(a), the trajectory begins in IR_1 and passes through IR_2 into IR_3. As the value of x_1 changes from increasing to decreasing, the trajectory enters DR_3. Along with the lower branch of a hysteresis, the trajectory returns through DR_2 into DR_1. Now, as the value of x_1 changes from decreasing to increasing, the trajectory re-enters IR_1. Let X_1 and X_2 be the points through which the trajectory enters IR_2 and IR_3 respectively. Let X_3 and X_4 be the points through which the trajectory leaves DR_3 and DR_2 respectively. These points (X_1, X_2, X_3 and X_4) are called switching points, since they locate the places where the linear systems change. Notice that there is no switching point for the trajectory from IR_3 to DR_3, since the linear systems in these two regions are the same. Similarly, there is no switching point from DR_1 to IR_1. Let t_1 be the travelling time of the trajectory (from X_1 to X_2) in region IR_2. Similarly, let t_2, t_3 and t_4 be the travelling times of the trajectory in regions $IR_3(DR_3)$, DR_2 and $DR_1(IR_1)$ respectively. The above procedure is then repeated, resulting in a set of new switching points X_1^1, X_2^1, X_3^1, X_4^1 and new values for the corresponding travelling times t_1^1, t_2^1, t_3^1, t_4^1. When the transients have diminished, we may observe a repetition of the switching points X_1, X_2, X_3, X_4 and the corresponding travelling times t_1, t_2, t_3, t_4 covering the entire region as shown in Figure 2(b). Then the steady state motion is classified as a period-one LCO. The frequency for this LCO can be determined by $f = 1/T$, where the period T is estimated by the sum of the travelling times (i.e., $T = t_1 + t_2 + t_3 + t_4$).

It is not necessary that the switching points and travelling times appear in the sequence as shown in Figure 2(b). For example, the steady state phase plane displayed in Figure 4(a) contains six switching points. The additional two points X_1^1 and X_2^1 are introduced after completing the sequence as discussed in the previous paragraph. In this case, a complete loop in the phase plane consists of six points $X_1, X_2, X_3, X_4, X_1^1, X_2^1$ and six corresponding travelling times $t_1, t_2, t_3, t_4, t_1^1, t_2^1$. Unlike the trajectory shown in Figure 2(b), a complete loop covering the entire region for this case also contains a smaller loop covering the two regions IR_1 and IR_2. The smaller loop is defined as the one that covers only one or two regions. The resulting LCO is of period-one, since we observe only one complete loop covering the entire region. However, the presence of a smaller loop indicates that the LCO has a harmonic component. Since the LCO is of period-one, the frequency is estimated by $f = 1/T$ with $T = t_1 + t_2 + t_3 + t_4 + t_1^1 + t_2^1$. The typical feature of LCO with harmonics can be verified by the appearance of four values for α when $\alpha' = 0$. Figure 4(b) shows a trajectory of period-one with harmonics, in which the smaller loop covers DR_2 and DR_3.

The point transformation method can be generalized in a straightforward manner to predict a period-n LCO or period-n LCO with harmonics (e.g., a period-two LCO with harmonics as shown in Figure 5(a) and a period-four LCO with harmonics as shown in Figure 5(b)), and the values of the frequency and maximum and minimum amplitudes can be estimated as well. If, however, after a sufficiently long time, the sequence of switching points still does not repeat, it may indicate that the motion is chaotic.

Based on the above discussion of applying the point transformation to the aeroelastic system with the hysteresis stiffness, we present two approaches in the following subsections.

2.1. FORMULATION 1

Starting from the initial point of a trajectory, this formulation is developed to determine the travelling times and the switching points in each region. First, the travelling times are determined by solving a non-linear equation. Then the switching points are calculated by the multiplication of a known matrix by a known vector. If the round-off error can be neglected, the formulation will produce the exact solution for the aeroelastic system. The detailed procedure is given as follows.

Step 0: Set the initial point $X_0 = (x_{01}, x_{02}, x_{03}, \ldots, x_{08})^{\mathrm{T}}$. If $x_{02} > 0$, set $i = 1$ for $\alpha_f \leqslant x_{01} \leqslant \alpha_f + \delta$, $i = 2$ for $x_{01} > \alpha_f + \delta$ and $i = 4$ for $x_{01} < \alpha_f$; otherwise set $i = 2$ for $x_{01} > -\alpha_f$, $i = 3$ for $-\alpha_f - \delta \leqslant x_{01} \leqslant -\alpha_f$ and $i = 4$ for $x_{01} < -\alpha_f - \delta$. Set $X_i = X_0$, and go to step i.

Step 1: Solve non-linear equations $\alpha_f + \delta = \{\mathrm{e}^{Ct} X_1 + \mathscr{C}(t) F_2\}|_{(1)}$ and $\alpha_f = \{\mathrm{e}^{Ct} X_1 + \mathscr{C}(t) F_2\}|_{(1)}$ separately for t. Here, $\{V\}|_{(n)}$ denotes the nth element of the vector V. Let the smallest positive solutions corresponding to the first and second equations be t^* and t^{**} respectively. If $t^* < t^{**}$, let $t_1 = t^*$, compute X_2 by $X_2 = \mathrm{e}^{Ct_1} X_1 + \mathscr{C}(t_1) F_2$, and go to step 2. If $t^{**} < t^*$, let $t_3 = t^{**}$, compute X_4 by $X_4 = \mathrm{e}^{Ct_3} X_1 + \mathscr{C}(t_3) F_2$, and go to step 4.

Step 2: First solve the non-linear equation $\{\mathrm{e}^{At} X_2 - \mathscr{A}(t) F_1\}|_{(2)} = 0$ for t, assign the smallest positive solution to t_u, and compute the maximum amplitude by $\alpha_{max} = \{\mathrm{e}^{At_u} X_2 - \mathscr{A}(t_u) F_1\}|_{(1)}$. Then solve the non-linear equation $-\alpha_f = \{\mathrm{e}^{At} X_2 - \mathscr{A}(t) F_1\}|_{(1)}$ for t, assign the smallest positive solution to t_2, and compute X_3 by $X_3 = \mathrm{e}^{At_2} X_2 - \mathscr{A}(t_2) F_1$. Go to step 3.

Step 3: Similar to step 1, solve $\alpha_f = \{\mathrm{e}^{Ct} X_3 + \mathscr{C}(t) F_2\}|_{(1)}$ and $\alpha_f + \delta = \{\mathrm{e}^{Ct} X_3 + \mathscr{C}(t) F_2\}|_{(1)}$ separately for t. Let the smallest positive solutions corresponding to the first and second non-linear equations be t^* and t^{**} respectively. If $t^* < t^{**}$, let $t_3 = t^*$, compute X_4 by $X_4 = \mathrm{e}^{Ct_3} X_3 + \mathscr{C}(t_3) F_2$, and go to step 4. If $t^{**} < t^*$, let $t_1 = t^{**}$, compute X_2 by $X_2 = \mathrm{e}^{Ct_1} X_3 + \mathscr{C}(t_1) F_2$, and go to step 2.

Step 4: Similar to step 2, first solve the non-linear equation $\{\mathrm{e}^{At} X_4 + \mathscr{A}(t) F_1\}|_{(2)} = 0$ for t, assign the smallest positive solution to t_l, and compute the minimum amplitude by $\alpha_{min} = \{\mathrm{e}^{At_l} X_4 + \mathscr{A}(t_l) F_1\}|_{(1)}$. Then solve the non-linear equation $\alpha_f = \{\mathrm{e}^{At} X_4 + \mathscr{A}(t) F_1\}|_{(1)}$ for t, assign the smallest positive solution to t_4, and compute X_1 *by* $X_1 = \mathrm{e}^{At_4} X_4 + \mathscr{A}(t_4) F_1$. Go to step 1.

The computations of e^{At} and $\mathscr{A}(t)$ can be found in Appendix C of reference [10]. $\mathscr{C}(t)$ is defined as $\mathscr{C}(t) = \int_0^t \mathrm{e}^{C(t-\tau)}\, \mathrm{d}\tau$. For various velocities, the matrix $\mathscr{C}$ may have one pair of complex and six distinct real eigenvalues, or two pairs of complex and four real eigenvalues. For the former case, the computations of e^{Ct} and $\mathscr{C}(t)$ are similar to those for e^{At} and $\mathscr{A}(t)$, while for the latter case, they are similar to those for e^{Bt} and $\mathscr{B}(t)$ in Appendix C of reference [10]. In fact, there are a number of ways to evaluate an exponential of a matrix, and 19 different methods are discussed by Moler and Van Loan [11]. Using the closed form for these computations yields an analytical formulation.

If no positive solution for the non-linear equation can be found, the motion either diverges if the linear system has at least one positive real part eigenvalue, or converges to the equilibrium if the real parts of all the eigenvalues of the linear system are negative. When all transients are diminished and a repetition in the values of the switching points is observed, the corresponding motion is an LCO. The amplitude and the period of the LCO can be predicted analytically. If after a sufficiently long time the repetition of the switching points cannot be found and the values of the switching points remain bounded, the motion may be classified as chaotic.

2.2. FORMULATION 2

This formulation applies only after transients die out and LCO appears. For example, for a period-one LCO, the four switching points can be written as (notice that the switching points are different from those correponding to a freeplay model):

$$X_1 = \begin{pmatrix} \alpha_f \\ s_1 \end{pmatrix}, \quad X_2 = \begin{pmatrix} \alpha_f + \delta \\ s_2 \end{pmatrix}, \quad X_3 = \begin{pmatrix} -\alpha_f \\ s_3 \end{pmatrix}, \quad X_4 = \begin{pmatrix} -\alpha_f - \delta \\ s_4 \end{pmatrix},$$

where s_1, s_2, s_3 and s_4 are seven-dimensional variable vectors representing the switching points in the subspace $\{X \in R^8 | x_1 = \alpha_f\}$, $\{X \in R^8 | x_1 = \alpha_f + \delta\}$, $\{X \in R^8 | x_1 = -\alpha_f\}$ and $\{X \in R^8 | x_1 = -\alpha_f - \delta\}$. Let t_i $(i = 1, 2, 3, 4)$ denote the corresponding travelling times. Then, t_i and $s_i (i = 1, 2, 3, 4)$ can be determined directly by solving the following system of non-linear equations:

$$X_2 = e^{Ct_1} X_1 + \mathscr{C}(t_1) F_4, \quad X_3 = e^{At_2} X_2 - \mathscr{A}(t_2) F_1, \quad X_4 = e^{Ct_3} X_3 - \mathscr{C}(t_3) F_4,$$
$$X_1 = e^{At_4} X_4 + \mathscr{A}(t_4) F_1. \tag{3}$$

Similar to a freeplay model, equation (3) can be reduced to a four-dimensional system with only the travelling times t_1, t_2, t_3 and t_4 as variables:

$$\alpha_f = \{H_1(t_1, t_2, t_3, t_4) G_1(t_1, t_2, t_3, t_4)\}|_{(1)}, \qquad \alpha_f + \delta = \{H_2(t_1, t_2, t_3, t_4) G_2(t_1, t_2, t_3, t_4)\}|_{(1)},$$
$$-\alpha_f = \{H_3(t_1, t_2, t_3, t_4) G_3(t_1, t_2, t_3, t_4)\}|_{(1)}, \qquad -\alpha_f - \delta = \{H_4(t_1, t_2, t_3, t_4) G_4(t_1, t_2, t_3, t_4)\}|_{(1)}, \tag{4}$$

where H_i $(i = 1, 2, 3, 4)$ are 8×8 matrix functions of t_1, t_2, t_3 and t_4, G_i $(i = 1, 2, 3, 4)$ are 8×1 vector functions of t_1, t_2, t_3 and t_4. However, the expressions for H_i and G_i are different from those for a freeplay model and they are defined in Appendix A.

The period is then given by $T = t_1 + t_2 + t_3 + t_4$ and the frequency $f = 1/T$. The amplitudes α_{max} and α_{min} of this period-one motion are given by

$$\text{solve } \{e^{At_u} X_2 - \mathscr{A}(t_u) F_1\}|_{(2)} = 0 \quad \text{for } t_u, \quad \alpha_{max} = \{e^{At_u} X_2 - \mathscr{A}(t_u) F_1\}|_{(1)},$$
$$\text{solve } \{e^{At_l} X_4 + \mathscr{A}(t_l) F_1\}|_{(2)} = 0 \quad \text{for } t_l, \quad \alpha_{min} = \{e^{At_l} X_4 + \mathscr{A}(t_l) F_1\}|_{(1)}, \tag{5}$$

where $X_2 = H_2(t_1, t_2, t_3, t_4) G_2(t_1, t_2, t_3, t_4)$ and $X_4 = H_4(t_1, t_2, t_3, t_4) G_4(t_1, t_2, t_3, t_4)$. Similar formulations can be derived for other types of LCOs.

Formulation 1 requires initial conditions to compute the switching points. It should be noted that this formulation is not a time-integration numerical scheme and the solution of each linear subsystem is determined analytically. The general formulation given in Section 2.1 can be used to detect any type of motion including period-n, period-n with harmonics, and chaotic motions. Under the same system parameters, starting from different initial conditions, the trajectory may converge to different LCOs, which indicates the coexistence of the LCOs of the original system (1).

When Formulation 2 is applied, only the steady state behavior is detected since no information with respect to the transient is recorded. This approach is more efficient if only the steady state solution is of interest. However, the formulations given in equations (4) and (5) are valid only for detecting a period-one motion. In order to detect other types of system motions, the formulation must be modified accordingly. Note that only the positive solutions (i.e., $t_i > 0$, $i = 1, 2, 3, 4$) to equation (4) are valid since the variables represent the travelling times. Also notice that one valid solution of equation (4) corresponds to one period-one LCO of the original aeroelastic system (1). However, there may be more than one valid solution to equation (4), indicating the coexistence of stable LCOs. However, Formulation 2 is not able to predict chaotic motion.

3. CASE STUDIES AND DISCUSSIONS

Applications of Formulations 1 and 2 are made to system (1) with the system parameters: $\mu = 100$, $a_h = -1/2$, $x_\alpha = 1/4$, $\zeta_\xi = \zeta_\alpha = 0$, $r_\alpha = 0{\cdot}5$, and $\bar{\omega} = 0{\cdot}2$. The pitch angle is

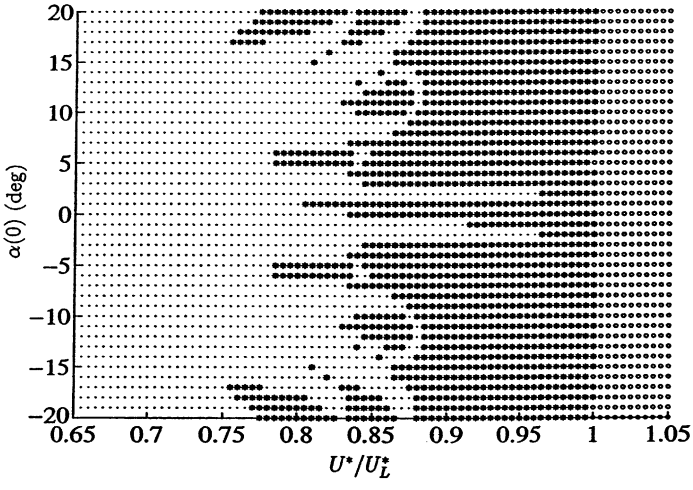

Figure 3. The flutter boundary diagram of an aeroelastic system with a hysteresis model; ●, damped motion; ★, LCO; ○, divergent motion.

TABLE 1

Case studies for hysteresis

Case	U^*/U_L^*	M_0	$x_1(0)$(deg)	Type of motion	T	α_{max}(deg)	α_{min}(deg)
1	0·80	0·5	1	p-1-h	98·6429	2·6826	− 2·4182
2	0·8097	0·5	1	p-1-h	99·0333	2·8342	− 2·4640
3	0·8098	0·5	1	p-2-h	200·6	2·8614	− 2·2844
4	0·81085	0·5	1	p-4-h	386·35	2·8646	− 2·4241
5	0·2	0·02	3	Chaotic			

hysteretic with $M(x_1)$ defined in equation (2) in which $M_0 = 0{\cdot}5$ or $0{\cdot}02^\circ$, $\delta = 1{\cdot}0^\circ$, and $\alpha_f = M_0 - 0{\cdot}5\delta$. The plunge is linear with $G(x_3) = x_3$. The formulations presented in the previous section do not depend on the choice of parameters. The system parameters and the hysteresis constants discussed in this section are chosen, so that the point transformation results can be compared with the numerical time-integration results reported by Chan [9].

The flutter boundary diagram shown in Figure 3 with several isolated pockets of LCOs inside the main flutter boundary is similar to that in Chan [9]. For velocity ratios $(U^*/U_L^*) > 1$, since the linear subsystems in all six regions have positive real parts, the system motions are divergent. As U^* decreases below U_L^*, the real parts of all eigenvalues of systems in IR_1, IR_3, DR_1, and DR_3 are negative, but some eigenvalues of the systems in IR_2 and DR_2 may have positive real parts, which results in various non-linear behavior: damped motion, LCO or chaotic motion. In the main LCO region, the point transformation method detects a pattern of four distinct switching points and two values of maximum and minimum values of α when $\alpha' = 0$ for the steady state, indicating a simple sinusoidal motion with a dominant frequency. For the motions on the inside LCO pockets, the harmonic components are detected and period-one, period-two and period-four LCOs are detected for various velocity ratios and initial conditions.

Several cases are selected for detailed discussion with results shown in Tables 1 and 2. Table 1 includes the cases of various LCOs and the period doubling phenomena leading to

TABLE 2

Coexistence of limit cycle oscillations

Case	U^*/U_L^*	$x_1(0)$(deg)	Type of motion	T	α_{max}(deg)	α_{min}(deg)
1	0·80	1	p-1-h	98·6429	2·6826	− 2·4182
2	0·80	5	p-1-h	98·6429	2·4182	− 2·6826

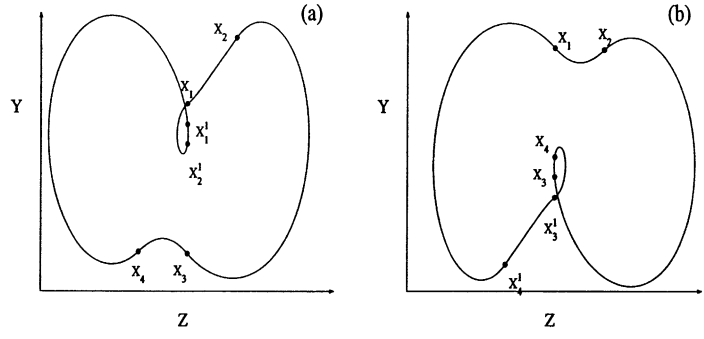

Figure 4. General trajectories for period-one with harmonics: (a) the smaller loop covers IR_1 and IR_2; (b) the smaller loop covers DR_1 and DR_2; ●, switching points.

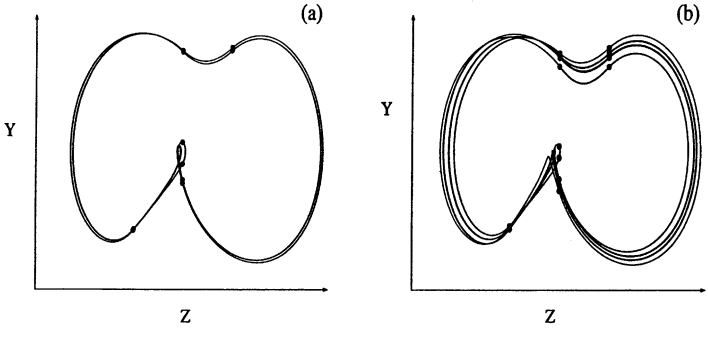

Figure 5. Trajectories for a period-two with harmonics (a) and a period-four with harmonics (b) LCOs; ●, switching points.

a chaotic motion, while Table 2 shows the coexistence of two distinct LCOs under the same system parameters but with different initial conditions. The initial values other than $x_1(0)$ are set to zero for the cases reported in Tables 1 and 2, and $M_0 = 0{\cdot}5^\circ$ for cases in Table 2. Notice that in Tables 1 and 2, "p-n" denotes "period-n motion", "p-n-h" denotes "period-n with harmonics motion", T represents the period, and α_{max} and α_{min} denote the absolute maximum and minimum values of the pitch angle. The results obtained by using Formulation 1 presented in Section 2.1 agree with those obtained by using Formulation 2, except for Case 5 in Table 1 since Formulation 2 cannot be used to predict chaos. Besides the tables, the results are also shown in Figures 4–9. Similar to the figures for a freeplay model reported in Part 1 of this study, the filled circles denote the predicted results obtained by using the formulations, and the solid lines represent the numerical solutions obtained by using the fourth order Runge–Kutta time-integration scheme.

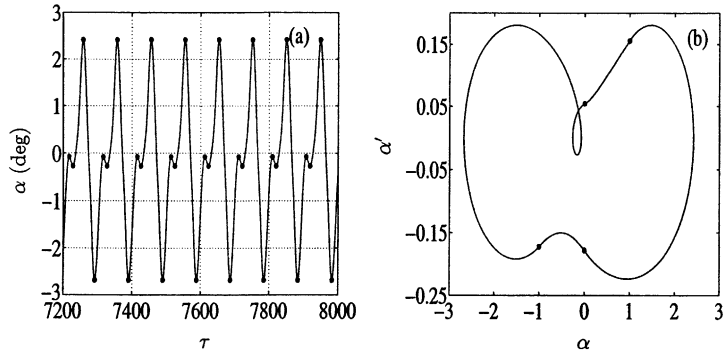

Figure 6. Case 1 in Table 1: (a) time history; (b) trajectory of α–α', ——, numerical result; ●, point transformation method.

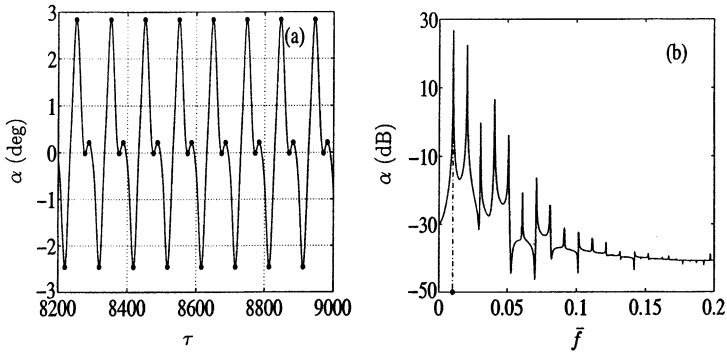

Figure 7. Case 2 in Table 1: (a) time history. (b) PSD plot; ——, numerical result; ●, point transformation method.

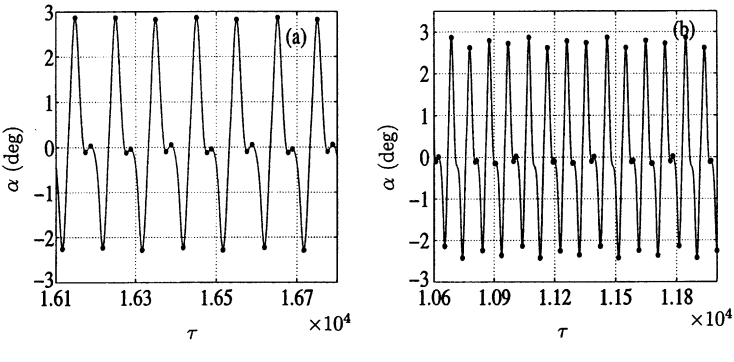

Figure 8. Time histories for Cases 3 and 4 in Table 1: (a) Case 3; (b) Case 4; ——, numerical result; ●, point transformation method.

For Case 1 in Table 1, starting with $\alpha(0) = 1^\circ$ and using Formulation 1, an LCO is detected after seven cycles. Four different switching points and the corresponding four travelling times are detected. From our discussion presented in section 2, this LCO is of period-one. However, four different values of α when $\alpha' = 0$ are detected. These maximum

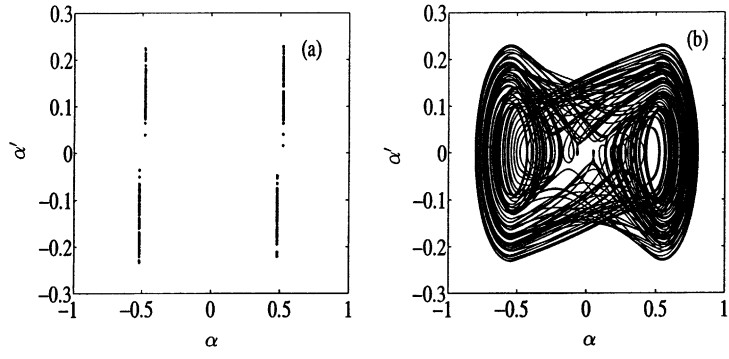

Figure 9. Case 5 in Table 1: (a) switching points; (b) phase projection of α–α'.

and minimum amplitudes of α are in good agreement with the time history obtained by using the fourth order Runge–Kutta scheme as shown in Figure 6(a). These four values of α, when $\alpha' = 0$ indicate the existence of a harmonic component. The trajectory of α–α' and the switching points are displayed in Figure 6(b). From the trajectory, we know that the complete loop covers the entire region once, and there is a smaller loop in region IR_1, indicating the existence of a harmonic component. Hence, the LCO of Case 1 is of period-one with harmonics. The frequency estimated by $f = 1/T = 1/98{\cdot}6433 = 0{\cdot}0101$ can be verified by the power spectral density (PSD) plot from the time history. In Case 2, six switching points, six travelling times and four different values of α when $\alpha' = 0$ are recorded after the transients diminished. The location of the switching points and the trajectory of α–α' are similar to those shown in Figure 4(a). As discussed in section 2, this LCO is classified as period-one with harmonics. The frequency $f = 1/T = 1/99{\cdot}0333 = 0{\cdot}0101$ agrees well with the dominant frequency reported from the PSD plot shown in Figure 7(b). The numerical solution and the maximum and minimum amplitudes of α when $\alpha' = 0$ are displayed in Figure 7(a). The total travelling time, $T = 200{\cdot}6$, in Case 3, is almost double the value $T = 99{\cdot}0333$ reported for Case 2. Both Formulations 1 and 2 indicate ten switching points and eight amplitudes of α when $\alpha' = 0$. Moreover, the switching points displayed in the trajectory are similar to those shown in Figure 5(a), where the complete loop covers the entire region twice, and it also contains smaller loops covering regions, DR_1 and DR_2. Hence, the resulting LCO is of period-two with harmonics. When the value of U^* increases to $0{\cdot}81085U_L^*$, a period-four with harmonic motion is found. Eighteen switching points and 14 amplitudes of α when $\alpha' = 0$ are found by using both formulations. The location of the switching points and the trajectory of α–α' are similar to Figure 5(b). Figures 8(a) and 8(b) present the pitch amplitudes corresponding to $\alpha' = 0$ for Cases 3 and 4 respectively.

By decreasing the value of M_0, a chaotic motion (Case 5) is detected. For this case, the values of switching points, travelling times and the amplitudes of α obtained using Formulation 1 do not settle down to a repeated sequence even after a very long time $\tau > 15\,000$. The values of the switching points appear to be on four vertical lines in the state space as shown in Figure 9(a). Notice that there are only two vertical lines corresponding to a chaotic motion in a typical freeplay model. This suggests that the motion is chaotic. The chaos is confirmed from the trajectory of α–α' (Figure 9(b)). The trajectory results from the numerical scheme, and a typical "two-well potential" trajectory is observed. The PSD plot from the numerical solution is similar to Figure 11(c) in reference [10] and also confirms the existence of broadband frequency components, an indication of chaos. This case has been carefully studied in reference [9].

Table 2 demonstrates the coexistence of stable limit cycles which correspond to $U^*/U_L^* = 0{\cdot}80$. Using Formulation 1, starting from $\alpha(0) = 1^\circ$ and 5°, the motions converge to two different period-one LCO with harmonics. The trajectories of α–α' and the switching points for Case 1 are displayed in Figure 6(b). For Case 2, the trajectory of α–α' and the switching points are similar to Figure 6(b) with a smaller loop in region DR_3. There are two sets of valid solutions to equation (4), namely $\{t_1 = 6{\cdot}31, t_2 = 55{\cdot}54, t_3 = 10{\cdot}96, t_4 = 25{\cdot}84\}$ and $\{t_1 = 10{\cdot}96,\ t_2 = 25{\cdot}84,\ t_3 = 6{\cdot}31,\ t_4 = 55{\cdot}54\}$, which correspond to Cases 1 and 2 respectively.

4. CONCLUDING REMARKS

A mathematical technique based on the point transformation method is introduced to investigate the dynamical response for a self-excited two-d.o.f. aeroelastic system with structural non-lienarity represented by a hysteresis stiffness. The method provides an accurate result since the solutions for the corresponding linear subsystems are determined accurately by using analytical techniques and the switching points where the change in linear regions occur are located exactly. Two formulations are developed, and they can be applied to predict the frequency and amplitude of LCOs. Moreover, the formulations are also capable of detecting complex aeroelastic behaviors such as the periodic motion with harmonics, period doubling, chaotic motions and the coexistence of stable limit cycles. The effectiveness of the proposed method has been demonstrated by verifying that the formulations can be used to predict the complex non-linear behaviors of an aeroelastic system with hysteresis non-linearity. The point transformation technique can also be extended for hysteresis stiffnesses in both d.o.f.

ACKNOWLEDGMENTS

The authors would like to acknowledge the support received from the Natural Sciences and Engineering Research Council of Canada.

REFERENCES

1. S. F. SHEN 1959 *Journal of Aerospace Science* **26**, 25–32. An approximate analysis of nonlinear flutter problems.
2. L. GONG, Y. S. WONG and B. H. K. LEE 1998 *Dynamics of Continuous, Discrete and Impulsive Systems* **4**, 99–119. Dynamics of a coupled system of Duffing's equations.
3. L. LIU, Y. S. WONG and B. H. K. LEE 2000 *Journal of Sound and Vibration* **234**, 641–659. Application of the centre manifold theory in nonlinear aeroelasticity.
4. S. J. PRICE, H. ALIGHANBERI and B. H. K. LEE 1995 *Journal of Fluids Structures* **9**, 175–193. The aeroelastic response of a two-dimensional airfoil with bilinear and cubic structural nonlinearities.
5. H. ALIGHANBARI and S. J. PRICE 1996 *Nonlinear Dynamics* **10**, 381–400. The post-Hopf-bifurcation response of an airfoil in incompressible two-dimensional flow.
6. D. S. WOOLSTON, H. L. RUNYAN and R. E. ANDREWS 1957 *Journal of Aeronautical Science* **24**, 57–63. An investigation of effects of certain types of structural nonlinearities on wing and control surface flutter.
7. S. F. SHEN and C. C. HSU 1958 *Journal of Aeronautical Science* **25**, 136–137. Analytical results of certain nonlinear flutter problems.
8. E. J. BREITBACH 1980 *NASA TP* 1620. Flutter analysis of an airplane with multiple structural nonlinearities in the control system.
9. Y. CHAN 1997 *National Research Council Canada, NRC Summer Student Project Report IAR*-97-1. Numerical simulation of a two-dimensional airfoil with a hysteresis non-linearity.

10. L. LIU, Y. S. WONG and B. H. K. LEE 2002 *Journal of Sound and Vibration* **253**, Nonlinear aeroelastic analysis using the point transformation method, Part I: for freeplay models.
11. C. MOLER and C. VAN LOAN 1978 *SIAM Review* **20**, 801–836. Nineteen dubious ways to compute the exponential of a matrix.

APPENDIX A: DEFINITIONS OF C_1, H_i AND G_i

$$C_1 = \begin{pmatrix} 0 & 1 & 0 & 0 \\ a_{21} & a_{22} & a_{23} + \mathrm{j}d_0\beta\left(\dfrac{\bar{\omega}}{U^*}\right)^2 & a_{24} \\ 0 & 0 & 0 & 1 \\ a_{41} & a_{42} & a_{43} - \mathrm{j}d_1\beta\left(\dfrac{\bar{\omega}}{U^*}\right)^2 & a_{44} \end{pmatrix},$$

$$H_1(t_1, t_2, t_3, t_4) = (I - \mathrm{e}^{At_4}\mathrm{e}^{Ct_3}\mathrm{e}^{At_2}\mathrm{e}^{Ct_1})^{-1}, \quad H_2(t_1, t_2, t_3, t_4) = (I - \mathrm{e}^{Ct_1}\mathrm{e}^{At_4}\mathrm{e}^{Ct_3}\mathrm{e}^{At_2})^{-1},$$
$$H_3(t_1, t_2, t_3, t_4) = (I - \mathrm{e}^{At_2}\mathrm{e}^{Ct_1}\mathrm{e}^{At_4}\mathrm{e}^{Ct_3})^{-1}, \quad H_4(t_1, t_2, t_3, t_4) = (I - \mathrm{e}^{Ct_3}\mathrm{e}^{At_2}\mathrm{e}^{Ct_1}\mathrm{e}^{At_4})^{-1},$$

where I denotes the identity 8×8 matrix.

$$\begin{aligned} G_1(t_1, t_2, t_3, t_4) = {} & \mathrm{e}^{At_4}\mathrm{e}^{Ct_3}\mathrm{e}^{At_2}\mathscr{C}(t_1)F_4 - \mathrm{e}^{At_4}\mathrm{e}^{Ct_3}\mathscr{A}(t_2)F_1 \\ & - \mathrm{e}^{At_4}\mathscr{C}(t_3)F_4 + \mathscr{A}(t_4)F_1, \\ G_2(t_1, t_2, t_3, t_4) = {} & -\mathrm{e}^{Ct_1}\mathrm{e}^{At_4}\mathrm{e}^{Ct_3}\mathscr{A}(t_2)F_1 - \mathrm{e}^{Ct_1}\mathrm{e}^{At_4}\mathscr{C}(t_3)F_4 \\ & + \mathrm{e}^{Ct_1}\mathscr{A}(t_4)F_1 + \mathscr{C}(t_1)F_4, \\ G_3(t_1, t_2, t_3, t_4) = {} & -\mathrm{e}^{At_2}\mathrm{e}^{Ct_1}\mathrm{e}^{At_4}\mathscr{C}(t_3)F_4 + \mathrm{e}^{At_2}\mathrm{e}^{Ct_1}\mathscr{A}(t_4)F_1 \\ & + \mathrm{e}^{At_2}\mathscr{C}(t_1)F_4 - \mathscr{A}(t_2)F_1, \\ G_4(t_1, t_2, t_3, t_4) = {} & \mathrm{e}^{Ct_3}\mathrm{e}^{At_2}\mathrm{e}^{Ct_1}\mathscr{A}(t_4)F_1 + \mathrm{e}^{Ct_3}\mathrm{e}^{At_2}\mathscr{C}(t_1)F_4 \\ & - \mathrm{e}^{Ct_3}\mathscr{A}(t_2)F_1 - \mathscr{C}(t_3)F_4. \end{aligned}$$